

# Space Efficient Sequence Alignment for SRAM-Based Computing: X-Drop on the Graphcore IPU

Luk Burchard\*  
luk@simula.no  
Simula Research Laboratory  
Oslo, Norway

Max Xiaohang Zhao\*  
max.zhao@charite.de  
Charité Universitätsmedizin  
Berlin, Germany

Johannes Langguth  
langguth@simula.no  
Simula Research Laboratory  
Oslo, Norway

Aydın Buluç  
abuluc@lbl.gov  
Lawrence Berkeley National  
Laboratory  
Berkeley, CA, USA

Giulia Guidi  
gg434@cornell.edu  
Cornell University  
Ithaca, NY, USA

## ABSTRACT

Dedicated accelerator hardware has become essential for processing AI-based workloads, leading to the rise of novel accelerator architectures. Furthermore, fundamental differences in memory architecture and parallelism have made these accelerators targets for scientific computing.

The sequence alignment problem is fundamental in bioinformatics; we have implemented the *X-Drop* algorithm, a heuristic method for pairwise alignment that reduces search space, on the Graphcore Intelligence Processor Unit (IPU) accelerator. The *X-Drop* algorithm has an irregular computational pattern, which makes it difficult to accelerate due to load balancing.

Here, we introduce a graph-based partitioning and queue-based batch system to improve load balancing. Our implementation achieves 10× speedup over a state-of-the-art GPU implementation and up to 4.65× compared to CPU. In addition, we introduce a memory-restricted *X-Drop* algorithm that reduces memory footprint by 55× and efficiently uses the IPU’s limited low-latency SRAM. This optimization further improves the strong scaling performance by 3.6×.

## 1 INTRODUCTION

Today’s architectures are complex but often suboptimal for modern irregular computation, being overprovisioned for arithmetic computation and challenging the programmer to cope with the high cost of moving data. A clear insight into this problem is provided by the Top500 list, in which the world’s 10 fastest machines achieve peak performance of up to 83% in the computationally intensive LINPACK benchmark but no more than 3% peak performance in the High-Performance Conjugate Gradient (HPCG) benchmark, which involves irregular computation [1].

In the last decade, the Graphics Processing Unit (GPU) has emerged as a leading architecture for high-performance computing (HPC) challenges involving dense linear algebra and scientific computing [2]. However, GPUs are single instruction multiple data (SIMD) architectures, and this can be a limitation for computational challenges that suffer from high load imbalance, as is often the case with data analytics and general computation. They require regular data access and work pattern to reach their theoretical peak performance [3]. A general-purpose processor such as a CPU is

better suited for non-uniform data access but does not provide the high instruction throughput achieved by GPUs, since CPUs are optimized for latency rather than throughput. Therefore, new architectures are needed for HPC that can provide more flexible acceleration like CPUs while providing high throughput like GPUs.

Recently, the Graphcore Intelligence Processing Unit (IPU), a massively parallel multiple instruction multiple data (MIMD) SRAM-based processor designed as an AI accelerator, has emerged as a potential solution to irregular computation by combining fine-grained memory access with wide parallelism [4]. While processors connected to external RAM are constrained by the von Neumann bottleneck, SRAM-based computing eschews complex memory hierarchies by providing sufficient SRAM storage on the processing chip to fit a problem instance [5]. IPUs were developed for AI applications but showed potential for other applications, such as for the breadth-first search algorithm, stencil computations, and cardiac simulation [6–8]. The question we seek to answer in this work is if new SRAM-based architectures can improve performance on a wider range of emerging HPC challenges, such as bioinformatics.

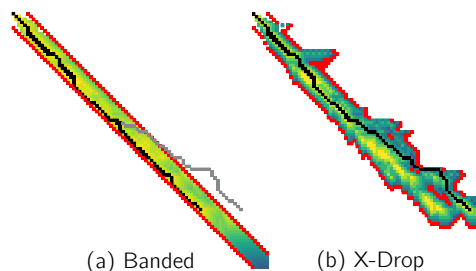


**Figure 1:** On the left, the alignment is forced to stay within the banded area regardless of the score, missing the optimal alignment (gray). On the right, when the score (yellow-blue)  $X$  goes below the current best score, the search is terminated (red boundary), and the optimal alignment (black) is returned.

In bioinformatics, pairwise sequence alignment is a fundamental technique used in many scenarios, such as genome assembly, phylogenetic analysis, protein structure prediction based on homology, and searching for similar sequences in databases [9]. Long-read sequencing technologies are increasingly available, producing sequences with an average length of about 15,000-30,000 base

\*Both authors contributed equally to this research.

pairs (bp). Longer sequences allow for more precise genome assembly [10] but they come with increased algorithmic complexity and computational cost. Therefore, there is a need for efficient algorithms that can handle long-read sequencing data.

The Needleman-Wunsch (NW) algorithm is used for finding the best global alignment, while the Smith-Waterman (SW) algorithm is used for finding the best local alignment. There is also a version of pairwise alignment called semi-global, where one side of the sequences is forced to align, but the other is not. However, finding the optimal solution for these algorithms requires quadratic time as a function of sequence length, which is inefficient for long sequences. The critical role that sequence alignment plays in understanding protein and DNA sequences has made it a focal point in attempts to optimize both algorithms and hardware [11]. In practice, assumptions can be made based on the input data and the type of computation desired to create heuristic algorithms with subquadratic runtimes.

A popular heuristic that we target in this work is called *X-Drop*. The *X-Drop* algorithm is a heuristic for restricting the search space of a semi-global alignment algorithm. It reduces the quadratic cost by dynamically searching only for a high-quality alignment and stopping the computation early when a good alignment is impossible. This allows for a more dynamic fit to the data than a static search space (Figure 1). It is a promising algorithm for long-read sequencing data because a good alignment can be found in nearly linear time. Genomic pipelines already use *X-Drop* and its variants *Y-Drop* and *Z-Drop* due to their good alignment quality and fast runtime [12–15].

In the literature, we only found one implementation of the *X-Drop* algorithm on GPUs [16], and one on Field Programmable Gate Arrays (FPGAs) [17], which can only run on DNA sequences (no protein sequences). However, *X-Drop* is widely implemented on CPUs [14, 15, 18]. In this paper, we present an implementation of the *X-Drop* algorithm on a novel AI accelerator hardware, the Graphcore IPU, that is suitable for both DNA and protein alignment. The proposed IPU-based approach provides a competitive solution for accelerating *X-Drop* on a wider range of problem instances compared to traditional CPUs and GPUs. Here we demonstrate the practicality of our implementation by integrating it into two distributed-memory pipelines with high alignment volumes: ELBA, a *de novo* long-read genome assembler [12, 19], and PASTIS, a protein similarity search engine [13]. Our implementation is tested on a variety of real-world data, reporting speedup over state-of-the-art CPU and GPU implementations. Our work thus demonstrates the potential of AI architectures to accelerate the pairwise alignment of long sequences and their suitability for irregular scientific computations.

IPUs and other SRAM-based devices, such as Cerebras hardware [20], rely on the MIMD paradigm and a large SRAM, making them more effective for handling irregular computation. In this work, we not only highlight the advantages of SRAM-based computing for scientific computing and the speedup achieved for the *X-Drop* algorithm but also show where these novel devices need progress to be widely deployed. For example, improving the IPU interconnect would lead to significantly cheaper host-to-device transfer times.

Our contributions are as follows:

- First, we demonstrate the first application of a cluster of Graphcore IPUs for high-performance processing of irregular genomic data.
- Then, we present a memory-restricted version of *X-Drop* which reduces the required memory by a factor of up to 55×. This enables the algorithm to run in the IPU’s SRAM memory.
- To solve the host-device communication bottleneck, to the best of our knowledge, we are the first to treat sequence comparisons as a graph and perform graph partitioning to reduce data transfer.
- Finally, we integrate our algorithm into ELBA and PASTIS, two state-of-the-art bioprocessing pipelines.

## 2 BACKGROUND

In this section, we first describe the architectural features of the Graphcore IPU and give a definition of the *X-Drop* pairwise alignment problem. Then, we briefly describe two biological pipelines that use *x-drop* alignment and into which we have integrated our approach.

### 2.1 Graphcore IPU

The Graphcore IPU is a massively parallel multiple instruction multiple data (MIMD) processor consisting of a large number of independent units called *tiles*. Each of these tiles has a core and a small amount of SRAM memory. Rather than serving as a cache, the SRAM memories of the individual tiles together form the device memory, eliminating the need for a traditional cache hierarchy.

**2.1.1 Hardware.** Three IPU generations have been released so far, called GC2, GC200, and BOW. The BOW differs from the GC200 only in its clock frequency. In this work, we use both the GC200 and the BOW. Both IPU models, the GC200 and the BOW, consist of 1472 tiles, each containing a core and 624 KB SRAM, which run at 1.33 GHz on the GC200 and at 1.85 GHz on the BOW. Each IPU core runs six concurrent threads in *temporal multithreading*, meaning that they are scheduled consecutively in a fixed order. The majority of IPU instructions, including loading and storing from local tile memory, take exactly six cycles. Thus, the 8832 threads can be considered independent cores running at one-sixth the original clock frequency with no instruction or memory latency. The total SRAM per IPU is 918 MB, which can be read with an aggregate memory bandwidth of 46.9 TB/s (GC200) or 65.2 TB/s (BOW). However, data not local to a core must be communicated between tiles via the IPU exchange network, which has an aggregate bandwidth of 7.83 TB/s (GC200) or 10.9 TB/s (BOW). The IPU alternates between computation and communication in a bulk-synchronous parallel (BSP) [21] manner with no overlap between phases.

Since the IPU is an accelerator that does not run its own operating system, it is dependent on a host machine. Unlike GPUs, whose CPU host is usually within the same machine, a group of IPUs is connected to the host node via 100 Gb/s Ethernet. This means that the number of IPUs per host can vary greatly.

Our GC200 test system contains 64 IPUs, but only one dual-socket Xeon-based server. Consequently, host-to-device transfers

can become a bottleneck. Four IPU are used together in an IPU-M2000 blade, which in turn can be combined into larger systems called IPU-PODs. The M2000 also contains up to 448 GB of DRAM memory, which it can access at a rate of about 20 GB/s. This memory, while too slow for most computations, can be used to buffer data from host-to-device transfers. The IPU’s themselves are connected in a ladder topology with a bisection bandwidth of 128 GB/s. In terms of power consumption, two IPU are comparable to a powerful GPU like the NVIDIA A100 or a pair of moderately powerful CPUs [22].

**2.1.2 Programmability.** Unlike other hardware accelerators, the IPU is a distributed memory system consisting of multiple tiles that use a direct memory write technique for communication.

Poplar is the C++ framework used to program the IPU at the lowest level. It is inspired by TensorFlow and the dataflow programming model, as high-level program flow is defined as a dataflow graph, where we can define a state as a *Tensor* and a transfer function as a *Vertex*. Code that executes in a vertex is called a codelet. One can think of a codelet as analogous to a CUDA kernel. To synchronize computation and data accesses, the IPU hardware supports the BSP programming model, which divides algorithm execution into level-synchronous supersteps with three phases: Compute, Exchange, and Synchronize.

In Poplar, each *Tensor* and *Vertex* must be mapped to a tile. The programmer must define input and output *Tensor* for the *Vertex*. The compiler uses the dataflow graph and vertex mapping to create a synchronized data exchange following the BSP pattern. A higher-level control flow can be introduced to select the next BSP superstep to execute. Unlike MPI, the data exchange does not need to be explicitly programmed.

## 2.2 X-Drop Pairwise Alignment

The comparison of biological sequences is important for a deeper understanding of the role and function of genetic areas and protein structures, but also for the construction of the genomic sequence itself. The genome consists of strings of nucleotides (adenine, thymine, guanine, cytosine), which code for protein sequences and contain additional regulatory information. Genomes cannot be sequenced in their entire length; current sequencing technologies can only read and output sequences that are significantly shorter than the entire genome. Therefore, we need sequence alignment to reconstruct whole genomes. For short-read technologies such as Illumina, the average sequence length is 100-250 nucleotides (or base pairs, bp). In newer long-read technologies such as Pacific Biosciences and Oxford Nanopore, the average read length can be more than 20,000 bp and up to several megabases, enabling the generation of highly continuous bacterial genomes [23]. Long-read technologies are highly promising as they can further improve our understanding of genomic structure [24]. Yet, they also present new computational challenges due to their longer length and higher error rates.

The optimal sequence alignment between two sequences can be found in quadratic time and linear space [25, 26] if we use the classical Smith-Waterman or Needleman-Wunsch algorithm for local and global alignment, respectively. The sequence alignment problem is defined as follows. Given two sequences  $\mathcal{H} = h_1, h_2, \dots, h_m$ ,  $\mathcal{V} = v_1, v_2, \dots, v_n$ , with  $|\mathcal{H}| = m$ ,  $|\mathcal{V}| = n$  we want to find the

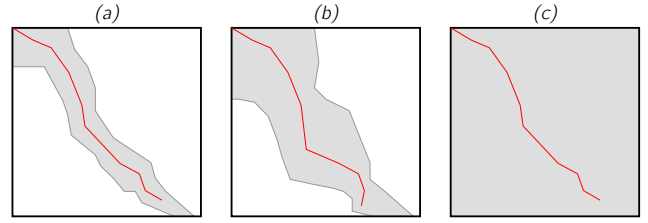


**Figure 2:** The red path is the optimal alignment, the gray area is calculated values, and the white area is non-calculated values. Due to the X-Drop condition, the white nonzeros contain a score of  $-\infty$ . Panel (a) shows an iteration with  $X = 10$ , (b) with  $X = 20$ , and (c) with  $X = \infty$ .

best scoring set of changes to transform sequence  $\mathcal{H}$  into  $\mathcal{V}$ . If we assume that the sequences are homologous, i.e. that they are evolutionarily related, the number of resulting changes is small. The alignment is done by dynamic programming, where we define a dense scoring matrix  $S(i, j)$ , with  $i \leq n$ ,  $j \leq m$ . The matrix  $S$  is filled from the upper left corner and extended to the lower right corner. In each nonzero, we store the best score for the alignment of each two-symbol pair  $(v_i, h_j)$ . This score is computed based on the match of  $v_i$  and  $h_j$  and the history of alignment for the previous three scores, as defined in the following rule:

$$S(i, j) = \begin{cases} S(i-1, j-1) + \text{Sim}(v_i, h_j) & \text{if } i > 0, j > 0, \\ S(i, j-1) + \text{gap} & \text{if } j > 0 \\ S(i-1, j) + \text{gap} & \text{if } i > 0 \end{cases}$$

In the above definition,  $\text{Sim}(v_i, h_j)$  is an arbitrary scoring function used to quantify the degree of similarity between a pair. In the case of DNA,  $\text{Sim}(v_i, h_j)$  is a positive value if  $v_i$  and  $h_j$  match (i.e., no change is required), or a negative value if they do not, and gap is also a negative value, meaning that either  $v_i$  or  $h_j$  has a symbol inserted or deleted at that position: The goal is to find a path of changes in  $S$  that maximizes the score and is optimal for aligning  $\mathcal{H}$  and  $\mathcal{V}$ . The scoring function assigns higher scores to likely biologically related sequences and lower scores to less likely related sequences.

In real-world scenarios, we can often make a reasonable assumption about where to find the optimal alignment on the two sequences, and this can lead to heuristics that can significantly reduce time and space complexity.

First, in one-to-many and many-to-many sequence alignment, the number of sequences to be compared can be reduced by first identifying common contiguous subsequences of fixed length  $k$  (i.e.,  $k$ -mers). The  $k$ -mer information reduces the number of sequences to be compared in large-scale computation but also gives us an indication of where in the sequences the optimal alignment might be found. This can lead to a semi-global alignment approach, where each pairwise alignment is divided into the left and right extension of the  $k$ -mer match.

The semi-global approach forces the alignment to start at one of the two extremities of the sequences (similar to the Needleman-Wunsch algorithm [27]), but leaves the other extremity free. This is a common approach first introduced by BLAST [14], and it can lead to shorter sequences, but it scales with  $O(mn)$ , where  $m$  and

$n$  are the lengths of the sequences involved since we still need to compute the entire matrix  $S$ .

The second key insight is that for sequences that have some similarity, the optimal alignment is often found on the diagonal of the  $S$  matrix, with the antidiagonal extremities storing low (i.e., bad) scores because the number of mismatches is high when moving away from the center of the diagonal, as shown in Figure 1. A common approach is to restrict the search to a predefined band region of  $S$  around the diagonal (left in Figure 1). This heuristic significantly reduces the time and space complexity but may restrict the search space too much and result in the failure to find the correct optimal alignment. This problem is particularly severe for sequences generated with long-read technologies, as these technologies are more prone to insertion and deletion of nucleotides (which can lead to a long gap sequence that moves the optimal alignment away from the diagonal) than to mismatches (which keep the optimal alignment mostly on the diagonal), which was the case with short-read technologies.

This provides the motivation for the  $X$ -Drop condition. The  $X$ -Drop strategy can be viewed as a dynamic band approach, where the search space is dynamically bounded by the score values rather than by a predefined band width. The  $X$ -Drop algorithm defines a threshold  $X$  that removes nonzeros (and the resulting possible path) from the  $S$  matrix that are worse than a path with the current best score. The assumption is that a path that is significantly worse (where significant is defined by  $X$ ) than the current best score is unlikely to lead to the optimal alignment. Let us denote the current best score as  $T$ . The  $X$ -Drop condition states that if  $S(i, j) < T - X$  in the current iteration of the dynamic program, then  $S(i, j) = -\infty$ .

The first iteration of the fill process for the  $X$ -Drop algorithm initiates in the upper left corner and initializes the matrix with  $S(0, 0) = 0$ . To avoid starting the alignment with a gap or gap sequence at a location in the matrix other than the upper left corner (i.e., where both sequences start), we define the off-matrix access as  $S(i, j) = -\infty, i < 0 \vee j < 0$ . This is because we want to perform a semi-global alignment and force one side of the extremities (from the  $k$ -mer match heuristic) to align. If  $X$  is large, the computation approaches filling the entire dynamic programming matrix  $S$ , whereas when  $X$  is small, the non-zeros in  $S$  are pruned as we move away from the optimal result, and these non-zeros become  $-\infty$ . In Figure 2 we show the impact of different  $X$  values on the search space of the scoring matrix.

The  $X$ -Drop algorithm has been widely implemented and variants used for commonly used long-read alignment software such as minimap2 [28]. In this work, we implemented the original  $X$ -Drop algorithm as formulated by Zhang [29, 30]. Their implementation traverses the dynamic programming matrix  $S$  in an antidiagonal fashion. They fill the non-zeros along the antidiagonal line from the upper right corner to the lower left corner of the dynamic programming matrix  $S$ . This sweeping anti-diagonal approach is initiated at  $S(0, 0)$  and progresses until the lower right corner is reached. To fill a cell in an antidiagonal of the matrix, only the scores of the adjacent cells (top, top-left, and left) are needed. These are stored in the antidiagonals that were filled in the previous two phases. Earlier literature [29, 30] used this insight to store only three antidiagonals: two for the previous phases and one for the current phase. This approach is popular for SIMD parallelism because the

dependencies for input and output non-zeros are well aligned. But this is not strictly necessary. Gotoh [31] stated that storing two antidiagonals is sufficient. However, it is not often used in practice because SIMD parallelism is difficult to achieve. Despite that, in this work, we choose to store only two antidiagonals as the IPU is a MIMD architecture, and we aim to reduce the memory footprint.

## 2.3 ELBA

ELBA is a long-read assembler implemented for distributed-memory parallelism that uses sparse matrices as the main data structures, mapping the *de novo* assembly process onto sparse matrix computation [19]. ELBA is composed of five main stages which comply with the Overlap-Layout-Consensus paradigm for assembling long-read sequencing data. In the first step,  $k$ -mer counting, the input sequences are parsed to extract subsequences of fixed length  $k$  and count their frequency. This produces a 1D distributed hash table of the  $k$ -mers and their frequencies and sequences of origin. This hash table is then transformed into a 2D  $|k\text{-mers}|\text{-by-}|sequences|$  sparse matrix that we call  $A^T$ . In the second step, called overlap detection, ELBA multiplies  $A$  by its transpose  $A^T$  to detect overlapping  $k$ -mer matches between input sequences. In this way, a  $|sequences|\text{-by-}|sequences|$  matrix  $C$  is obtained in which the non-zeros represent such matches and their position on the sequences. Then, for each non-zero of  $C$ , the  $X$ -Drop pairwise alignment algorithm is run, starting from the  $k$ -mer match position, to obtain similarity values and remove false matches from the matrix. In the fourth and fifth stages, ELBA simplifies the matrix, that is the assembly graph, to extract contiguous areas of the genomes (i.e., *contigs*), which are the result of the assembly process.

## 2.4 PASTIS

PASTIS [13] similar to ELBA computes protein homology searches as a distributed sparse matrix multiplication. PASTIS computes the  $k$ -mer count and  $AA^T$ , but then must perform additional matrix multiplication with the matrix  $S$  to produce the output  $|sequences|\text{-by-}|sequences|$  matrix. The  $S$  matrix is called the substitution matrix and is used to find quasi-exact  $k$ -mer matches because it has been shown that strictly enforcing exact matches in protein homology searches can lead to a significant loss of accuracy. Thus, the overlap detection phase has the form of  $ASA^T$ . Once the output matrix is formed, PASTIS computes an alignment step on each non-zero, similar to ELBA. PASTIS has two alignment modes: seed-and-extend with  $X$ -Drop and Smith-Waterman alignment. Using  $X$ -Drop, PASTIS initiates the alignment from the  $k$ -mer match.

Both PASTIS and ELBA defer implementation of  $X$ -Drop to the Library for Sequence Analysis (SeqAn) C++ library for CPU [18]. ELBA also provides support for the GPU-based  $X$ -Drop alignment called LOGAN [16]. LOGAN does not support protein alignment.

## 3 ALGORITHM

In this section, we describe the algorithm we implemented on the Graphcore IPU and the algorithmic changes we made to make the computation more suitable for the IPU.

One of the major challenges in implementing sequence alignment on specialized hardware is the memory requirement since storing the entire dynamic matrix can exceed the available memory.

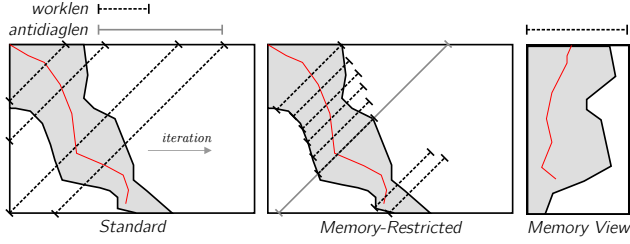


**Figure 3:** The antidiagonal length is  $\delta = \min(|\mathcal{H}|, |\mathcal{V}|)$ . The memory-restricted version allocates work memory of  $\max_k |U_k - L_k| \leq \delta_b \leq \delta$ . The left panel illustrates the standard algorithm ( $3\delta$  memory). The middle one illustrates our algorithm ( $2\delta_b$  memory), while the right one is the pattern of our memory usage over time.

In Section 2.2, we described how it is possible to reduce the memory footprint of the scoring matrix  $S$  by storing only three antidiagonal phases (the previous two phases and the current phase  $k$ ) to traverse  $S$ , instead of storing the entire matrix. It can be observed that an antidiagonal can never become larger than  $\delta = \min(|\mathcal{H}|, |\mathcal{V}|)$ , where  $\mathcal{H}$  and  $\mathcal{V}$  are the sequences involved in the alignment. To limit the workload, it is common to use a lower  $L_k$  and an upper bound  $U_k$  for the antidiagonal, where  $|U_k - L_k|$  is the length of the antidiagonal in iteration  $k$ . These boundaries are derived from the number of scores in  $S$  that are not yet  $-\infty$  (i.e., scores that have not triggered the X-Drop termination condition).

To store three antidiagonal phases, we need  $3\delta$  of memory for each alignment run. This memory requirement is too high for the IPU. Therefore, we address this problem with a two-step approach. First, we reformulate the algorithm using the technique found in [31] to store only two antidiagonal phases. This is possible by using a temporary variable since the values in the antidiagonal  $k$  and  $k - 2$  are one iteration offset accessed and written. In addition, we propose to use a band in the iteration, which is different from the classical banded algorithm shown in Figure 1 on the left, because the band is not static in space (i.e., it does not remain fixed around the diagonal), but is constantly realigned to the active iteration position that stores the best score. It is possible to observe that even though the antidiagonal is fully allocated ( $\delta$ ), only a small part of it is accessed during each phase  $k$ , since  $|U_k - L_k| \leq \delta$ . Therefore, in our implementation, we assume a bound length  $\delta_b$ , which is the total working length  $w = \max_k |U_k - L_k|$  of the antidiagonal to keep  $w \leq \delta_b \leq \delta$ . Thus, we use the restricted  $\delta_b$  to constrain the algorithm in memory by placing antidiagonals in the active working area of the algorithm, resulting in a memory allocation of  $2\delta_b$ . Figure 3 on the left illustrates the antidiagonal length (black dashed line) for the original algorithm, while the middle one illustrates the antidiagonal length for our proposed memory-restricted version. The gray area is part of the scoring matrix  $S$  filled by the X-Drop algorithm. The right panel in Figure 3 illustrates a reinterpretation of the iteration space of the working memory region. The choice of an appropriate  $\delta_b$  value is related to the error rate of the sequence and the X-Drop factor. Both high error rates and large  $X$  increase the working length  $w$ , as shown in Section 6.1.

Algorithm 1 describes our memory-restricted algorithm using only two antidiagonals  $A_1, A_2$  of length  $\delta_b$ .  $T$  is the best score

found by the algorithm, while  $L, U$  are the lower and upper iteration boundaries, respectively. It is worth remembering that the algorithm for aligning X-Drop is semi-global; one side of the extremities of the two sequences is forced to align while the other side is left free. This is the case because each alignment results from splitting two sequences into four sequences (i.e., two for the left extension and two for the right extension) using the  $k$ -mer seed match information. To perform the forward alignment (right extension) from left to right. For the backward alignment (left extension), we use an index transformation  $op(\cdot)$  that produces either forward or backward accesses to  $\mathcal{H}$  and  $\mathcal{V}$ . This way, we do not have to completely reverse the sequences to perform the alignment with the left extension. The current diagonal iteration is given by  $k$ . The algorithm terminates when  $L$  and  $U$  converge, i.e., when no values greater than  $-\infty$  remain in the working set of the algorithm.

**Algorithm 1** The memory-restricted X-Drop algorithm.

```

1:  $L, U, T', T, k \leftarrow 0$ 
2:  $L1_{inc}, L2_{inc} \leftarrow 0$ 
3:  $A_1, A_2 \leftarrow \{-\infty, \dots, -\infty\}$ 
4:  $A_1[0] \leftarrow 0$ 
5: while  $L \leq U + 1$  increase  $k$  by 1 and do
6:    $W_2 \leftarrow A_2 + (-L + L2_{inc})$   $\triangleright$  C-style array offsetting
7:    $W_1 \leftarrow A_1 + (-L + L2_{inc} + L1_{inc})$ 
8:    $W'_1 \leftarrow A_1 + (-L)$ 
9:    $w_{last} \leftarrow W_1[L - 1]$   $\triangleright$  Instead of a third anti-diagonal
10:  while  $i \in (L, \dots, U + 1)$  do
11:     $j \leftarrow k - i - 1$ 
12:     $w_{new} \leftarrow W_1[i]$ 
13:     $score \leftarrow \max \left\{ \begin{array}{l} W_2[i] - gap \\ W_2[i - 1] - gap \\ w_{last} + sim(\mathcal{H}[op(i)], \mathcal{V}[op(j)]) \end{array} \right\}$ 
14:     $w_{last} \leftarrow w_{new}$ 
15:    if  $score < T - X$  then
16:       $score \leftarrow -\infty$ 
17:    end if
18:     $W'_1[i] \leftarrow score$ 
19:     $T' \leftarrow \max\{T', score\}$ 
20:  end while
21:   $L_{prev} \leftarrow L$   $\triangleright$  zero t1 shifted values
22:   $L \leftarrow \max(k + 1 - N, \operatorname{argmin}(W'_1 \neq -\infty))$ 
23:   $U \leftarrow \min(|\mathcal{H}| - 1, \operatorname{argmax}(W'_1 \neq -\infty) + 1)$ 
24:   $L1_{inc} \leftarrow L - L_{prev}$ 
25:   $T \leftarrow T'$ 
26:   $swap(A_1, A_2)$ 
27:   $swap(L1_{inc}, L2_{inc})$ 
28: end while

```

## 4 IMPLEMENTATION

In this section, we describe the implementation of the memory-restricted X-Drop algorithm on the Graphcore IPU accelerator.

Our implementation focuses on large sequences (both protein and DNA) whose length is in the range of 1K to 25K. This raises two challenges that we address in this work. First, the memory requirement for each alignment is large, given that a single pairwise

**Table 1:** Optimizations implemented and described throughout Section 4.4.

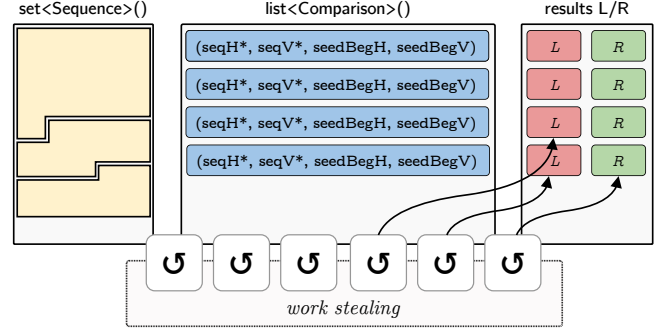
	Optimization	Time [ms]	GCUPS	To Prev.	Total
15% error	Single tile	493907	5.00		
	Scale to 1472 tiles	414	6034	1194×	1193.8×
	Use 6 threads	87	28705	4.76×	5679.4×
	LR splitting	85	29163	1.02×	5768.0×
	Work-stealing	85	29084	1.00×	5765.8×
	Dual issue	65	37933	1.30×	7504.9×
ELBA Ecoli	Single tile	4180499	14.52		
	Scale to 1472 tiles	6939	7302	602×	602.4×
	Use 6 threads	2707	14860	2.56×	1543.9×
	LR splitting	2470	16828	1.10×	1692.3×
	Work-stealing	1713	21935	1.44×	2440.4×
	Dual issue	1268	28587	1.35×	3296.8×

alignment is executed on a single tile of the IPU, where that tile has 624 KB of addressable memory and six threads, each of which requires space for the algorithm. So we need to be able to allocate 6× the amount of working memory during the alignment on one tile. Second, due to the IPU’s BSP (bulk synchronous parallel) architecture, we need to create a load-balanced problem (i.e., with equal runtime for each tile) to use all tiles equally. If a single tile takes more time, all other tiles must wait, resulting in poor utilization of hardware resources.

#### 4.1 Kernel Architecture

The *X-Drop* kernel was written as a Poplar vertex (codelet) in C++, where Poplar is the equivalent of CUDA for IPU. Our implementation focuses on using the six hardware threads of each IPU tile. In the absence of synchronization instructions such as atomics or mutexes, we implemented a data-parallel implementation with throughput in mind. It is possible to perform tile-local coarse-grained synchronization by combining the hardware threads into a single supervised thread, which can use the entire set of six threads on a single alignment. However, this would result in context switches for each synchronized part of the algorithm, which would degrade performance. Therefore, we choose to have each thread perform a single performance alignment, and for this reason we have a sixfold memory footprint on each tile.

The IPU’s inability for random external memory access and the limitation of a single tile to 624 KB of local memory forces us to choose a memory minimizing algorithm that enables many input sequences to be stored on a tile in order to maximize the number and size of sequences that can be processed on a single tile. To optimize the use of limited local memory, our tile architecture employs several techniques that allow all six threads to be used during the execution of the *X-Drop* algorithm. By reducing the amount of memory needed to implement the memory-restricted algorithm and efficiently using the available processing resources, we can achieve better performance and efficiency in sequence alignment on the IPU. The optimizations we implemented and their relative improvement are summarized in Table 1, measured for real-world and synthetic data.

**Figure 4:** Tile structure with six worker threads filling in the output for left and right seed extension, using work stealing. The input is sequences and a list of seed extension information.

**4.1.1 Tile Data Structures.** The tile receives as input a set of sequences *seqs* and a list of seeds for these sequences to be computed. The seed matches are tuples containing a pointer to two sequences in *seqs*, and the position of the seeds on them to avoid having to split the sequences on the host, as shown in Figure 4. The output array stores a list of tuples for each left and right extension of a seed. Our representation has many advantages over state-of-the-art seed extension representation, as no preprocessing has to be done on the host device. Our algorithm can operate in reverse on continuous memory by providing a suitable *op* function for Algorithm 1. Furthermore, in real-world pipelines, a pair of sequences often must be aligned considering multiple seed matches, which would lead to the retransmission of the same sequences, negatively affecting performance. Thanks to the detached structure for sequences and seed alignment information we introduced, we can transfer multiple seed matches and sequences at once. This optimization saves  $O(\#seeds)$  in data transfer from the host to the device. The use of the *op* function is useful because the sequences can be truncated at different positions for the left and right extension, creating  $\#matches \times 4 \mathcal{H}_L, \mathcal{H}_R, \mathcal{V}_L, \mathcal{V}_R$  individual sequences.

**4.1.2 Left and Right (LR) Extension Splitting.** Scaling from one thread to six threads per tile, we expect a speedup of 6×. However, the observed speedup is only 4.7×. This is because only 5 comparisons with 10 unique sequences have the memory to accommodate large sequences of length 10,000 bp on a single tile, leaving one of six threads without work. To use all threads, we introduce a finer distribution of work by having threads work individually on the left and right extensions of the seed matches rather than assigning both extensions to the same thread. This doubles the number of work units to be distributed so that each thread is used for large sequences instead of leaving one thread idle. Our synthetic data, whose sequences are generated to be of equal length, does not benefit from this optimization because if we have 5 uniform workloads (i.e., sequence comparisons), they are split into 10 uniform workload units. This leaves four threads with two workload units, as is the case even without this optimization since we rely on BSP synchronization, which does not benefit from an unbalanced workload since the bottleneck is caused by the longest-running process. Nevertheless, this optimization can lead to a significant

improvement in real-world workload due to a larger variance in seed position and sequence length.

**4.1.3 Eventual Work Stealing.** Despite the LR optimization to increase workload granularity, we can still observe a large variance in thread runtime due to sequence length variance in real data. Using a simple round-robin workload allocation will leave one or more threads without work, resulting in load imbalance. Since synchronization is not possible on the IPU tiles, except for coarse thread joining, we initially resorted to statically assigning work to individual threads. However, since a single-seed extension has a relatively high runtime, we decided to implement *Eventual Work Stealing*. A work-stealing approach makes it possible for an idle thread to take a unit of work from the globally stored list of seed extensions and work on it locally. Since no mutexes were available to ensure that only one thread at a time could access the seed structure, we resorted to globally swapping a value. This does not avoid race conditions, but in this case, we would only compute a seed extension multiple times and not skip over it. Since instruction latencies are deterministic, two threads stealing the same unit of work will perpetually continue to do so. We introduced a small thread-unique busy wait loop to create variance, eventually avoiding this race condition and a possible perpetual joint execution. This loop reduces the race conditions from 16K to 18 for a total number of 1.13M alignments performed.

**4.1.4 Dual Instruction Issuing.** The tiles implement a Very Long Instruction Word (VLIW) ISA with dual instruction issuance on two lock-synchronous pipelines, one integer and one floating point. The instructions require a single cycle to retire, except for certain floating-point operations such as `exp`, `log`, `sqrt`, which are not used in our code. Thus, we are not concerned with lock synchronicity. The integer pipeline is responsible for memory and branching operations, while the floating point pipeline is only responsible for floating point arithmetic.

We analyzed the generated assembly and found that registers in the integer pipeline in the inner loop of the X-Drop algorithm spilled when traversing the antidiagonal. Therefore, we reformulated our similarity function *Sim* (Section 2) to return floating-point values, forcing a floating-point representation of our scores to make use of additional floating-point registers. In addition, we used a compiler hint to use the built-in floating-point max instruction.

## 4.2 Batching

Before the kernel is executed, the sequences must be distributed (in pairs) to the individual tiles. This distribution can be modeled as a  $k$ -partitioning problem, where each comparison task is assigned to a particular tile and the total number of tiles is  $k$ . The size of each comparison is equal to the sum of the lengths of the two sequences involved. Given the BSP pattern of the IPU, it is important to minimize the longest-running tile runtime, which may cause other tiles to wait.

Estimating computational complexity is difficult because perfectly matched sequences have a smaller search space (they do not deviate too much from the diagonal) than sequences with higher mismatch rates. However, completely mismatching sequences run faster because the computation terminates early due to the X-Drop

condition triggered by rapidly increasing bad scores. Therefore, we use the maximum running time, which is quadratic to the lengths of the sequences involved, for each comparison as an estimate of the computation time.

## 4.3 Graph Based Sequence Partitioning

A single seed extension  $e_c$  with comparison index  $c$  for two sequences  $\mathcal{H}, \mathcal{V} \in \Omega$ , where  $\Omega$  is the total set of input sequences, stores the following information  $e_c := (\mathcal{H}, \mathcal{V}, \mathcal{H}_s, \mathcal{V}_s)_c \in \mathcal{C}$ , where  $\mathcal{H}_s, \mathcal{V}_s$  refer to the initial position of the seed on the two sequences  $\mathcal{H}, \mathcal{V}$ , respectively. In previous work, the relationship between pairs of sequences was not considered (e.g., when two identical sequences have multiple  $k$ -mer matches), but these  $c$ -tuples were considered as single sequence extensions to be computed.

In this work, we propose to interpret the set of seed extensions as a graph partitioning problem to reduce the number of data transfers between the host and the IPU. The idea is to reduce the transmission of the same sequence of  $\Omega$  shared by multiple  $e_c$  sent to the IPU in the same batch. Since memory is not shared between tiles and communication must be determined at compile time, we are limited to reusing sequences on a single tile. Dynamic compilation of IPU exchanges at runtime takes too much time. Therefore, we cannot create dynamic sequence exchanges and keep  $\Omega$  entirely on the IPU. Reuse of many sequences is enabled by our tile data structures, which store the local set of sequences  $\omega_i \subset \Omega$  detached from the set of seed extensions in a tile with index  $i$ . The set of seed extensions stores only a reference to the sequences in  $\omega_i$ .

Real-world bioinformatics pipelines, which rely on many-to-many sequence comparisons, store information about which sequences need to be aligned against each other, which can benefit our optimization. Both ELBA and PASTIS provide this information in a sparse matrix representation that includes planned sequence alignments. Here, we propose a graph partitioning algorithm to increase data reuse. Given a graph  $G(V, E)$  with  $V \subseteq \Omega$ ,  $V$  the set of vertices (i.e., sequences), we want to distribute the set of edges  $e_j \in E$  that is representative of the seed extensions (i.e., alignments) to be performed. The graph has an edge between two vertices where a comparison uses the sequences represented in  $V$ . We partition our graph into partitions  $p_i$  containing a set of edges and the associated set of sequences unique to the tile. The partitions are constrained to hold sequences whose total size is less than or equal to the available tile memory.

To avoid this immediate optimization step taking a lot of time, we partition the graph using a greedy strategy to stay within a tight time frame, which is usually less than one second for our tested data. The greedy strategy is given as follows. Take a vertex in the graph and walk linearly through the edge list. Add the starting vertex to the partition and the adjacent vertex to the edge. Continue to walk through the edges and add the adjacent vertex to the partition until adding a new vertex would exceed the memory limit of the partition; start a new partition. For simplicity, we leave the batching of our partitions to our batching algorithm.

For sequences of the same length, this optimization achieves a sequence reuse effectiveness of  $2\times$ , since for each new comparison on a tile, only one new sequence has to be transmitted, since the other is already in  $\omega_i$ . In a real world scenario, however, the length

**Table 2:** Data sets for comparisons with CPU and GPU implementations with distribution for the left and right extensions.

Name	Cmp Count	SeqLen Avg	SeqLen P10 L	SeqLen Avg L	SeqLen P90 L	SeqLen P10 R	SeqLen Avg R	SeqLen P90 R	Complexity Avg
simulated85	40 000	9 992	9 992	9 992	9 992	9 991	9 991	9 991	99 830 072
ecoli	568 208	7 319	832	7 322	13 684	823	7 317	13 675	45 870 449
ecoli100	15 611 769	3 631	431	3 705	8 319	388	3 557	8 087	12 524 999
elegans	16 794 715	7 346	1 184	7 347	13 375	1 179	7 345	13 380	52 763 834

of the sequences can vary significantly. Thus, for *E. coli* and *C. elegans*, we observed that we could pack up to 41 smaller sequences into a single large sequence, which drastically improved the transfer performance.

#### 4.4 Multi-IPU Support

The use of multiple IPUs is a critical factor in achieving optimal performance under a large computational load, as is often the case with many-to-many sequence alignment. We have several options to scale our algorithm. One of these options is the combined multi-device approach, which provides a virtual, seemingly homogeneously extended IPU with a larger number of tiles. However, it should be noted that this approach can lead to global synchronization and requires larger batches, resulting in suboptimal parallelization efficiency. Therefore, we opted for a different approach using multiple individual IPU devices. With our load balancing driver, we can effectively manage load balancing and schedule alignments between connected standalone devices. It is worth mentioning that the individual devices remain hidden from the user. With such a method, we can achieve better performance while ensuring optimal resource utilization.

Our wrapping driver class manages the Poplar graph and enables execution on multiple IPUs. The driver class handles the submission of batches and takes care of the internal distribution of work between IPUs and their respective tiles. Batches are submitted to a work queue that is shared among all IPU instances. The shared queue is connected to the input stream of each IPU, which allows prefetching by the IPU since all submitted batches are fully pre-processed. Prefetching on the IPU allows data transmission to be interleaved with computation allowing us to hide transmission time to an extent.

## 5 EXPERIMENTAL SETUP

Our tests were performed on three large systems. First, we used the Perlmutter supercomputer, where each node is equipped with a single-socket AMD EPYC 7763 CPU, 256 GB RAM, and four NVIDIA A100 (Ampere) GPUs. Second, IPU results for the Mk2 IPUs were obtained on the ex3 supercomputer, which has a dual-socket Intel Xeon Platinum 8168 CPU connected to 16 Mk2 blades, each containing four IPU GC200s. Third, our IPU BOW results were collected on a Paperspace Cloud instance with a dual-socket AMD EPYC 7742 CPU and 425 GB RAM, connected to 16 BOW IPUS in two blades. The experiments were compiled with native optimizations, and AVX2 was explicitly enabled with GCC 11.2.0.

### 5.1 Comparison to State-of-the-Art

To demonstrate the impact of our work, we compared our implementation to CPU -based implementations SeqAn [18, 32], ksw2 [15, 28],

libgaba [28], and genomertools [33]. All implementations were integrated into our benchmark runner program, which implements parallel processing of alignments using OpenMP [34]. Several datasets extracted from ELBA (Table 2) and a synthetic dataset were tested with  $X \in \{5, 10, 15, 20\}$ .

For our performance measurements, we define giga-cell updates per second (GCUPS) as a metric to evaluate the performance of the tools on a given data set. Cells are defined as the number of fields in the dynamic programming matrix  $S$  corresponding to the theoretical number of cells. The time to perform a complete alignment by computing  $S$  is measured by the total time  $t$ . Heuristics, such as an  $X$  factor or banding, reduce the number of cells actually computed. We define our metric as:  $GCUPS = \frac{|H| \times |V|}{t}$ . The execution time was measured for our IPU implementation using the number of cycles required to compute the alignment on the device. The number of cycles to execute a given program is deterministic if the input and configuration parameters are identical. Using the tile’s frequency  $f = 1.33 \times 10^9$  for the IPU Mk2 and  $f = 1.85 \times 10^9$  for the IPU Bow, the total on-device execution time can be derived by  $t = \text{cycles}/f$ . On the GPU, the on-device execution performance was measured by measuring the kernel execution time without data transfer in LOGAN. On the CPU, the execution time for the alignments is measured without the preparation time required for loading sequences and comparison metadata.

**5.1.1 Strong Scaling.** Using the *E. coli 100x* and *C. elegans* data defined in Table 2, we investigated the strong scaling performance of our approach, scaling a single BOW IPU to 32 IPUs. Each scaling experiment was performed with graph-based partitioning (Section 4.3) enabled and disabled. Total execution time was measured after the alignments were generated, excluding loading times for the sequences.

### 5.2 Data Set

For the standalone experiments, we generated synthetic data and extracted realistic data from the ELBA pipeline to evaluate the performance of our own implementation as a function of certain properties of the data sets. The datasets, including distribution characteristics, used to compare the different  $X$ -Drop implementations are listed in Table 2.

The distribution of our data indicates a lower sequence length of 5 kb for *E. coli 100x* compared to 15 kb for *E. coli*, and *C. elegans*. Relative seed position on the read is relatively evenly distributed along the sequence length in our data, with a greater slope toward the center and edges in the *E. coli* and *C. elegans* datasets. In *E. coli 100x*, we observed that the left and right extensions are skewed toward lower complexity alignment. Synthetic datasets were generated with equal sequence length and fixed read similarity. Mismatches were generated by uniform-randomly mutating individual bases outside the seed position. ELBA datasets were based on alignments

generated during processing of PacBio SMRT HiFi read data from *E. coli* (29x and 291x) and *C. elegans* (40x) in the alignment step of the pipeline with a seed length of 17 in all datasets. [16]

### 5.3 Real-World Application

For the two real pipelines PASTIS (Section 2.4) and ELBA (Section 2.3), we perform the IPU experiments on the IPU BOW system. Scaling to multiple IPU was transparently enabled by setting the NUMBER\_IPUS parameter of our library. Therefore, no further code optimization was required in either pipeline. Both pipelines create sparse *overlap* matrices to determine the sequences to be compared. We interpret these matrices as adjacency matrices for our graph partitioning scheme presented in Section 4.3.

To compare the system performance of our systems, we focus only on the *alignment* step, since the other nodes are not equipped with corresponding hardware. The other phases of the pipelines are not affected by the device on which the alignment step is performed. Any speedup that one method provides over the other contributes to the speedup of the entire pipeline relative to the percentage of time that the alignment step originally took.

**5.3.1 PASTIS.** Our integration is based on the git-commit fced0f2, in which we replaced the SeqAn library X-Drop alignment algorithm with our own implementation of X-Drop. PASTIS does not provide a X-Drop GPU algorithm because, to our knowledge, no GPU X-Drop algorithm is implemented for protein alignment. For PASTIS, the largest dataset we could run was a uniformly subsampled protein database from the metaclust [35] dataset containing 500 k protein sequences. We used an X-Drop factor of  $X = 49$  and a gap penalty of  $-2$  and used BLOSUM62 [36] as our similarity matrix, as described by Selvitopi et al. [13]. Further, we choose a  $k$ -mer length of 6, with two required seed matches per overlap.

**5.3.2 ELBA.** The results are based on the git-commit of the GPU branch 40c1b3a. We used the same input data provided by Guidi et al. [19] to measure performance. Comparisons were made with *E. coli* and *C. elegans*. We compared the runtime of the alignment kernel in the ELBA bioinformatics pipeline. Experiments were performed with X-Drop factors of {10, 15, 20} and a  $k$ -mer length of 31, with two required seed matches per overlap.

## 6 EXPERIMENTAL RESULTS

In this section, we describe the outcomes and performance of our design choices and implementation, and compare them to the state-of-the-art.

### 6.1 Selection of $\delta_b$

To test the validity of our algorithm’s assumption that  $\delta_w$  is significantly smaller than  $\delta$ , we performed experiments on different synthetic datasets with decreasing similarity rates from 100% down to 0% at sequence lengths of 20000 base pairs, as shown in Figure 6. In this empirical test, we found that the working band  $\delta_w$  is smallest for perfectly matching sequences, except for sequences that are completely mismatched at a similarity of 0%. For perfectly matching sequences, the computed band is small. The highest score is always on the diagonal and the search is terminated near the diagonal based on  $X$ .

In the cases where the similarity decreases to 80%, the working band doubles for small  $X$  and increases only to 13% for  $X = 100$ . The X-Drop values studied reach a maximum bandwidth when the sequence mismatch is about 70%. As the similarity decreases further, the bandwidth decreases again because the computation terminates early due to the X-Drop condition. For fully mismatched sequences with a similarity of 0%, the range of computed cells is limited by  $X$  to a distance from the beginning of both sequences depending on the mismatch and gap penalties.

For real-world *E. coli* data,  $\delta_w$  values were {176, 339, 656} for realistic values of  $X$  of {10, 15, 30}. Compared to the longest sequence length required for  $\delta$ , we can choose a  $\delta_b \geq \delta_w$ , which saves up to 98.2% of memory for a realistic  $X$  value of 15.

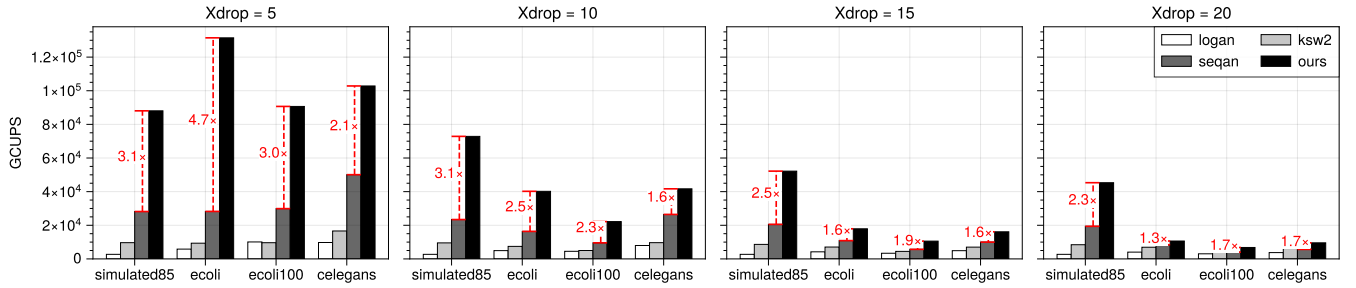
### 6.2 Comparison to State-of-the-Art

Overall, the IPU implementation shows better performance, while the smallest difference was observed for *E. coli* and  $X = 20$  as illustrated in Figure 5. The single IPU performance on the device reaches 102,844 GCUPS with *C. elegans* at  $X = 5$ , which is 2.05× faster than that of SeqAn (50,084 GCUPS) and 10.54× faster than LOGAN (9,761 GCUPS) on a single GPU. For  $X = 20$ , the IPU is 1.68× faster than SeqAn and 2.55× faster than LOGAN.

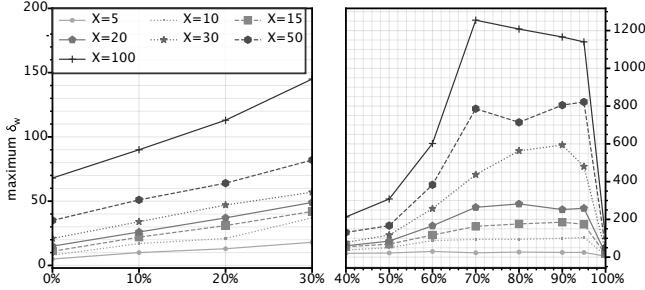
Of the CPU implementations, the implementation of SeqAn X-Drop consistently performs better than ksw2 because ksw2 [15] penalizes long gaps less, resulting in a larger search space. In addition, tests on an Intel Xeon Platinum 8360Y showed consistently worse performance than the AMD EPYC 7763; therefore, we have omitted the results here. LOGAN generally does not perform well on HiFi data, and we attribute this to higher sequence similarity and a more unbalanced length distribution for smaller values of  $X$ . In our implementation, we find that larger  $X$  values extend the computational work to similar sequences, while dissimilar sequences continue to end early. This leads to faster-decreasing performance for more dissimilar input sequences. In comparison, the SIMT implementation of LOGAN gains performance over other hardware because it has a larger search space.

Figure 7 illustrates the strong scaling from 1 to 32 IPU devices for  $X \in \{5, 10, 15, 20, 50\}$  on *E. coli 100x* and *C. elegans*. Scaling is nearly linear up to 16 IPU for larger  $X \geq 15$  with up to 15 *times* speedup on 16 devices on *C. elegans* ( $X = 50$ ). Apart from a constant speedup due to the higher clock frequency of the IPU Bow, the scaling properties do not differ significantly between the IPU Bow and IPU Mk2 systems tested. Unless otherwise stated, the scaling results refer to the IPU Mk2 system.

Graph partitioning of comparisons allows sequences to be reused for multiple comparisons. This reduces the amount of sequence data that must be transmitted to the IPU and increases the number of comparisons that can be performed on a single IPU tile. For the *E. coli 100x* dataset, the number of batches decreases by  $-52\%$  (816 to 387), and for the *C. elegans* dataset, the number of batches decreases by  $-44\%$  (1,723 to 972). On both data sets, this increases performance. Using  $X = 10$ , for *E. coli 100x* 1.46× on a single device and up to 3.59× using 32 devices and for *C. elegans* 1.29× on a single device and 1.83× on 32 devices. For higher  $X = 20$  and  $X = 50$ , scaling is linear up to 16 and 32 devices, both single and multiple comparisons. or  $X = 50$  using multi-comparisons is 1.18× faster



**Figure 5:** Normalized performance of our IPU implementation on 4 data sets (Table 2) in comparison to CPU implementations SeqAn, ksw2 and GPU implementation LOGAN. The relative speedup to the second fastest implementation SeqAn is given.



**Figure 6:** Find the maximum spread of the upper and lower pointers of the antidiagonal  $\delta_w$  for error rates from 0% to 100% symbol mismatches with varying X-Drop values.

on the *E. coli 100x* dataset using 1 device and 1.55 $\times$  faster using 32 devices. This indicates a higher computational load per batch, allowing more IPUs to be fully utilized before the interconnect to the IPUs is saturated.

### 6.3 Real World Pipelines

The CPU and GPU results were collected on AMD EPYC 7763 nodes, while the IPU results were collected on the IPU BOW system with an AMD EPYC 7742.

**6.3.1 ELBA.** For *E. coli*, a single IPU required 7.4 seconds to perform the alignment phase with  $X = 15$ . Our implementation showed good scaling up to 8 IPUs, which reduced the alignment time to 2.2 seconds. Scaling to more devices was restricted by the small data set. The CPU system required 11.61 seconds with a single node, while the GPU code ran with up to 4 GPUs and required 52.14 seconds in the alignment phase. Then, we used the *C. elegans* data set, the largest data set we could run, which occupied around 400 Gb of the host system’s DRAM. Since the EPYC 7763 nodes have less memory, we compared the IPU with four CPU nodes and four GPU nodes. Using a CPU setup with four nodes, we achieved 227.5, 340.7 seconds for  $X$  of {15, 20}. GPU results were measured with a total of 16 GPUs, resulting in 1,068 seconds for  $X = 15$ . The IPUs alignment phase took 255.6 and 401.9 seconds for  $X$  of {15, 20}. For  $X \geq 15$ , we observed scaling up to 16 IPUs. The overall alignment runtime achieved a speedup of 22.3 $\times$  for a cluster of 16 GPUs and a speedup of 4.7 $\times$  for a four-node CPU cluster.

**6.3.2 PASTIS.** For PASTIS, we measured 44.9 seconds for the alignment step on the CPU, while the IPU required 9.6 seconds, which

corresponds to a 4.7 $\times$  speedup. Larger inputs with more than 500 k sequences resulted in segmentation faults, making larger-scale experiments infeasible. This is due to the large packets combined with the 32-bit MPI APIs, as we use a single rank with many CPU threads. This is true for both the IPU and CPU.

## 7 RELATED WORK

The literature on accelerating the Smith-Waterman and Needleman-Wunsch algorithms for sequence alignment is extensive [37–40]. The classical sequence alignment problem without additional heuristics computes the entire dynamic programming matrix for alignment. Other work has focused on accelerating specific tools and applications, including BLAST [41–43] and BWA [44], both of which implement heuristic alignment strategies. The data-intensive computational patterns in sequence alignment have led to the development of memory-centric processor architectures, including Processing in Memory (PIM) [45–48] and near-memory computing [49] systems. Edit-distance algorithms consider only the number of changes required to convert one sequence to another, with each change, whether an insertion, deletion, or substitution, incurring the same cost. This much more restricted formulation of an alignment problem has similar complexity properties of  $O(nm)$ . The Bitap-Algorithm [50] uses a bitmask and bitwise operations on a constrained alphabet to compute the edit distance between a pattern and a queried string. It was adapted with a greedy windowing heuristic for long sequences and parallelized execution in GenASM and Scrooge [51, 52], reducing the alignment complexity to  $O(n + m)$ , while also allowing for non-optimal alignment results.

The X-Drop algorithm for alignment has rarely been the target of hardware acceleration work. Recent efforts include GPU [16] and FPGA (Field Programmable Gate Array) [17], which surpassed the state-of-the-art CPU implementations at the time.

## 8 CONCLUSION

The processing power of modern CPUs has far outpaced the speed improvement of persistent and random access memory (DRAM), widening the gap between memory and processor performance. This discrepancy is masked by a highly hierarchical cache system in traditional CPUs. The Graphcore IPU’s single level of large, low-latency SRAM reflects the recent trend toward shifting computation to memory, in both PIM and near-memory computing approaches.

In this work, we implement the X-Drop sequence alignment algorithm on the Graphcore IPU. A massively parallel MIMD AI accelerator with a single level of low latency SRAM for storage. Our

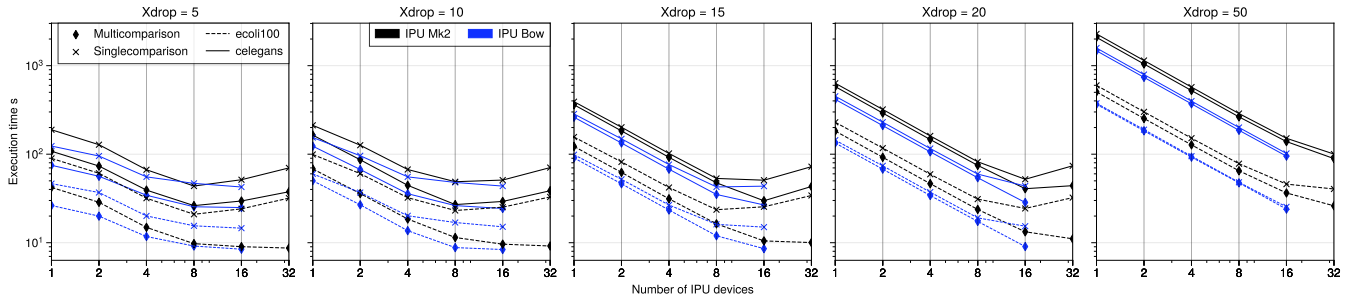


**Figure 7:** Scaling performance measured in execution time of alignment on *E. coli 100x* and *C. elegans* using 1 to 32 IPU devices. *Multicomparison* enables the use of a graph-based partitioning of comparisons that allows the reuse of sequences.

contributions include algorithmic updates to the X-Drop algorithm to adapt it to the memory-constrained IPU architecture. Our dynamic band restriction algorithm reduces memory usage without compromising alignment computation with real data. Our formulation of graph-based sequence partitioning enables the reuse of sequences in many-to-many sequence alignment settings common to genome assembly and protein cluster pipelines.

Our implementation of X-Drop sequence alignment outperforms current state-of-the-art implementations on CPU and GPU for both DNA and protein alignment for realistic  $X$  values. In addition, we demonstrate near-linear strong scaling properties on common IPU host configurations. In two real-world pipelines, ELBA and PASTIS, we show significant speedup using our IPU implementation as the algorithm for the X-Drop aligner.

Finally, we note that the low bandwidth of host-device communication and the rigidity of the BSP paradigm, as well as the lack of atomic operators for thread-level cooperative multitasking, are the major limitations of the Graphcore IPU system. Our implementation mitigates these issues, but future SRAM-based architecture should be improved to enable the widespread use of SRAM-based computing for more data-intensive computation.

In summary, the IPU has significant potential for accelerating irregular computations where low-level parallelism is difficult to exploit on highly instruction-parallel architectures such as GPUs.

## REFERENCES

- [1] H. Meuer et al. Top500 supercomputer sites, 2001.
- [2] M. Véstias and H. Neto. Trends of CPU, GPU and FPGA for high-performance computing. In *2014 24th International Conference on Field Programmable Logic and Applications (FPL)*, pp. 1–6, September 2014.
- [3] V. W. Lee et al. Debunking the 100X GPU vs. CPU myth: An evaluation of throughput computing on CPU and GPU. In *Proceedings of the 37th Annual International Symposium on Computer Architecture, ISCA '10*, pp. 451–460, New York, NY, USA, June 2010. Association for Computing Machinery.
- [4] Z. Jia et al. Dissecting the Graphcore IPU Architecture via Microbenchmarking, December 2019.
- [5] S. Mittal et al. A survey of SRAM-based in-memory computing techniques and applications. *Journal of Systems Architecture*, 119:102276, October 2021.
- [6] L. Burchard et al. Ipuq: Accelerating breadth-first graph traversals using many-core graphcore ipus. In *High Performance Computing: 36th International Conference, ISC High Performance 2021, Virtual Event, June 24–July 2, 2021, Proceedings*, pp. 291–309. Springer, 2021.
- [7] L. Burchard et al. Enabling Unstructured-Mesh Computation on Massively Tiled AI-Processors: An Example of Accelerating In-Silico Cardiac Simulation. *Frontiers in Physics*, 11:105, 2023.
- [8] T. Louw and S. McIntosh-Smith. Using the Graphcore IPU for traditional HPC applications. In *3rd Workshop on Accelerated Machine Learning (AccML)*, 2021.
- [9] A. Apostolico and R. Giancarlo. Sequence Alignment in Molecular Biology. *Journal of Computational Biology*, 5(2):173–196, January 1998.
- [10] S. L. Amarasinghe et al. Opportunities and challenges in long-read sequencing data analysis. *Genome Biology*, 21(1):30, February 2020.
- [11] M. Alser et al. Technology dictates algorithms: Recent developments in read alignment. *Genome Biology*, 22(1):249, August 2021.
- [12] G. Guidi et al. Parallel String Graph Construction and Transitive Reduction for De Novo Genome Assembly, October 2020.
- [13] O. Selvitopi et al. Distributed many-to-many protein sequence alignment using sparse matrices. In *SC20: International Conference for High Performance Computing, Networking, Storage and Analysis*, pp. 1–14. IEEE, 2020.
- [14] S. F. Altschul et al. Basic local alignment search tool. *Journal of Molecular Biology*, 215(3):403–410, October 1990.
- [15] H. Li. Minimap2: Pairwise alignment for nucleotide sequences. *Bioinformatics*, 34(18):3094–3100, September 2018.
- [16] A. Zeni et al. LOGAN: High-Performance GPU-Based X-Drop Long-Read Alignment. In *2020 IEEE International Parallel and Distributed Processing Symposium (IPDPS)*, pp. 462–471, New Orleans, LA, USA, May 2020. IEEE.
- [17] A. Zeni et al. The Importance of Being X-Drop: High Performance Genome Alignment on Reconfigurable Hardware. In *2021 IEEE 29th Annual International Symposium on Field-Programmable Custom Computing Machines (FCCM)*, pp. 133–141, May 2021.
- [18] K. Reinert et al. The SeqAn C++ template library for efficient sequence analysis: A resource for programmers. *Journal of Biotechnology*, 261:157–168, November 2017.
- [19] G. Guidi et al. Distributed-memory parallel contig generation for de novo long-read genome assembly. In *Proceedings of the 51st International Conference on Parallel Processing*, pp. 1–11, 2022.
- [20] G. Lauterbach. The Path to Successful Wafer-Scale Integration: The Cerebras Story. *IEEE Micro*, 41(6):52–57, November 2021.
- [21] L. G. Valiant. A bridging model for parallel computation. *Communications of the ACM*, 33(8):103–111, 1990.
- [22] S. Knowles. Graphcore. In *2021 IEEE Hot Chips 33 Symposium (HCS)*, pp. 1–25. IEEE, 2021.
- [23] M. Sereika et al. Oxford Nanopore R10.4 long-read sequencing enables the generation of near-finished bacterial genomes from pure cultures and metagenomes without short-read or reference polishing. *Nature Methods*, 19(7):823–826, July 2022.
- [24] S. Nurk et al. The complete sequence of a human genome. *Science*, 376(6588):44–53, April 2022.
- [25] D. S. Hirschberg. A linear space algorithm for computing maximal common subsequences. *Communications of the ACM*, 18(6):341–343, June 1975.
- [26] E. W. Myers and W. Miller. Optimal alignments in linear space. *Bioinformatics*, 4(1):11–17, March 1988.
- [27] S. B. Needleman and C. D. Wunsch. A general method applicable to the search for similarities in the amino acid sequence of two proteins. *Journal of Molecular Biology*, 48(3):443–453, March 1970.
- [28] H. Suzuki and M. Kasahara. Introducing difference recurrence relations for faster semi-global alignment of long sequences. *BMC Bioinformatics*, 19(1):45, February 2018.
- [29] Z. Zhang et al. Alignments Without Low-Scoring Regions. *Journal of Computational Biology*, 5(2):197–210, January 1998.
- [30] Z. Zhang et al. A Greedy Algorithm for Aligning DNA Sequences. *Journal of Computational Biology*, 7(1-2):203–214, February 2000.
- [31] O. Gotoh. An improved algorithm for matching biological sequences. *Journal of Molecular Biology*, 162(3):705–708, December 1982.
- [32] R. Rahn et al. Generic accelerated sequence alignment in SeqAn using vectorization and multi-threading. *Bioinformatics*, 34(20):3437–3445, October 2018.
- [33] G. Gremme et al. GenomeTools: A comprehensive software library for efficient processing of structured genome annotations. *IEEE/ACM transactions on computational biology and bioinformatics*, 10(3):645–656, 2013.

- [34] L. Dagum and R. Menon. OpenMP: An industry standard API for shared-memory programming. *IEEE Computational Science and Engineering*, 5(1):46–55, January 1998.
- [35] M. Steinegger and J. Söding. Clustering huge protein sequence sets in linear time. *Nature communications*, 9(1):2542, 2018.
- [36] S. Henikoff and J. G. Henikoff. Amino acid substitution matrices from protein blocks. *Proceedings of the National Academy of Sciences of the United States of America*, 89(22):10915–10919, November 1992.
- [37] Y. Liu et al. CUDASW++ 3.0: Accelerating Smith-Waterman protein database search by coupling CPU and GPU SIMD instructions. *BMC Bioinformatics*, 14(1):117, April 2013.
- [38] Z. Feng et al. Accelerating Long Read Alignment on Three Processors. In *Proceedings of the 48th International Conference on Parallel Processing*, pp. 1–10, Kyoto Japan, August 2019. ACM.
- [39] M. G. Awan et al. ADEPT: A domain independent sequence alignment strategy for gpu architectures. *BMC Bioinformatics*, 21(1):406, September 2020.
- [40] A. Müller et al. AnySeq/GPU: A novel approach for faster sequence alignment on GPUs. In *Proceedings of the 36th ACM International Conference on Supercomputing, ICS '22*, pp. 1–11, New York, NY, USA, June 2022. Association for Computing Machinery.
- [41] W. Ye et al. H-BLAST: A fast protein sequence alignment toolkit on heterogeneous computers with GPUs. *Bioinformatics*, 33(8):1130–1138, April 2017.
- [42] P. D. Vouzis and N. V. Sahinidis. GPU-BLAST: Using graphics processors to accelerate protein sequence alignment. *Bioinformatics (Oxford, England)*, 27(2):182–188, January 2011.
- [43] C. Ling and K. Benkrid. Design and implementation of a CUDA-compatible GPU-based core for gapped BLAST algorithm. *Procedia Computer Science*, 1(1):495–504, May 2010.
- [44] C.-M. Liu et al. SOAP3: Ultra-fast GPU-based parallel alignment tool for short reads. *Bioinformatics (Oxford, England)*, 28(6):878–879, March 2012.
- [45] O. Mutlu et al. A Modern Primer on Processing in Memory, August 2022.
- [46] W. Xu et al. RAPIDx: High-performance ReRAM Processing in-Memory Accelerator for Sequence Alignment. *IEEE Transactions on Computer-Aided Design of Integrated Circuits and Systems*, pp. 1–1, 2023.
- [47] S. Gupta et al. RAPID: A ReRAM Processing in-Memory Architecture for DNA Sequence Alignment. In *2019 IEEE/ACM International Symposium on Low Power Electronics and Design (ISLPED)*, pp. 1–6, July 2019.
- [48] F. Zokaee et al. Aligner: A Process-in-Memory Architecture for Short Read Alignment in ReRAMs. *IEEE Computer Architecture Letters*, 17(2):237–240, July 2018.
- [49] G. Singh et al. FPGA-Based Near-Memory Acceleration of Modern Data-Intensive Applications. *IEEE Micro*, 41(4):39–48, July 2021.
- [50] B. Dömölki. An algorithm for syntactical analysis. *Computational Linguistics*, 3(29-46):151, 1964.
- [51] D. S. Cali et al. GenASM: A High-Performance, Low-Power Approximate String Matching Acceleration Framework for Genome Sequence Analysis, September 2020.
- [52] J. Lindegger et al. Scrooge: A Fast and Memory-Frugal Genomic Sequence Aligner for CPUs, GPUs, and ASICs. *Bioinformatics*, pp. btad151, March 2023.